Materials Transactions, Vol. 64, No. 10 (2023) pp. 2346 to 2360

Heterostructured Materials by Severe Plastic Deformation: Overview and Perspectives

Liliana Romero-Resendiz[1,2,*], Muhammad Naeem[3,4,*] and Yuntian Theodore Zhu[1]

[1]*Department of Materials Science and Engineering, Mechanical Behavior Division of Shenyang National Laboratory of Materials Science, City University of Hong Kong, Kowloon, Hong Kong*
[2]*Facultad de Química, Departamento de Ingeniería Metalúrgica, Universidad Nacional Autónoma de México, Mexico City, 04510, Mexico*
[3]*Department of Physics, City University of Hong Kong, Kowloon, Hong Kong*
[4]*School of Metallurgy and Materials, University of Birmingham, Birmingham B15 2TT, UK*

Heterostructured materials (HSMs) constitute heterogeneously distributed soft and hard zones with a mismatch in mechanical or physical properties of at least 100% between them. A synergistic effect resulting from the interactive coupling between the heterogeneous zones surpasses the properties predicted by the rule of mixtures. Therefore, the mechanical or physical properties of HSMs are not achievable by their homogeneous counterparts. HSM production commonly requires plastic deformation to refine the microstructure and subsequent partial recrystallization heat-treatments to obtain heterogeneous distributions of grain size, texture, or defect density. Other routes are by applying surface plastic deformation or by stacking layers with a high property mismatch between them. All of those routes can be achieved by severe plastic deformation (SPD) techniques. This overview focuses on describing the fundamentals of HSMs produced by SPD. A critical description of the physics of SPD and HSMs, as well as the factors influencing their microstructural evolution, perspectives, and outstanding issues, are included. A critical comparison of the strength–ductility relationship in HSMs produced by different SPD techniques is also included to guide upcoming research. This overview is intended to serve as a basis for understanding and designing future HSMs produced by SPD.
[doi:10.2320/matertrans.MT-MF2022010]

(Received January 25, 2023; Accepted May 2, 2023; Published August 25, 2023)

Keywords: *severe plastic deformation, heterostructured materials, microstructure, mechanical properties*

1. Introduction

Heterostructured materials (HSMs) provide a positive answer to the tough question faced by the metallurgical community: is it possible to significantly increase both the strength and the strain-hardening to avoid the "inevitable" loss of ductility? Due to the above, HSMs constitute a fast-emerging field characterized by a significant contribution of hetero-deformation induced (HDI) strengthening. Since the coining of the term HDI strengthening and its in-depth description by Zhu *et al.* in 2019,[1] HSMs have inspired numerous multidisciplinary materials with outstanding mechanical performance.[2–5]

Unlike homogeneous materials, the HSMs require specific features for significant activation of HDI strengthening. Those features are mainly i) the coexistence of a soft and a hard zone with a mechanical mismatch of at least 100% between them to encourage strain partitioning, ii) an effective mutual constraining between zones, and iii) planar slip promoted mainly by low stacking fault energy (SFE) or short-range ordering (SRO).[2] As a result, geometrically necessary dislocation (GND) pile-ups form near the soft/hard interfaces to accommodate the strain mismatch. The GND pile-ups generate back stress in soft regions and forward stress in the harder ones. The combined contribution of both back and forward stress is known as HDI stress. While back stress provides hardening to the soft regions; forward stress promotes the deformation of hard zones. HSMs provide a successful strategy to reduce the strength–ductility trade-off of homogeneous materials.[6]

*Corresponding authors, E-mail: liliana.rom7@comunidad.unam.mx; m.naeem@bham.ac.uk

Besides their outstanding mechanical behavior, HSMs also have the processing advantage of being feasible by numerous thermo-mechanical routes, most of which are conducive to large-scale and low-cost industrial production. In many cases, HSMs require a combination of plastic deformation with partial recrystallization heat-treatments to encourage abnormal grain size growth or multiphase microstructures.[2] Severe plastic deformation (SPD) techniques are one of the routes that make it possible to combine with heat-treatments to produce HSMs (Fig. 1).

As shown in Fig. 1, SPD techniques can boost mechanical properties of metallic materials by an extensive grain refinement up to the nanometer scale.[3] However, the near simple shear deformation mode, which is characteristic of SPD techniques, produces mainly homogeneous microstructures that suffer from strength–ductility trade-off,[7] which can be overcome by the HSM strategy.[2,7–9] Thus, combining the virtues of SPD to produce HSMs is promising as a further step to obtain heterogenous microstructures, whether by grain size, multiphases, or crystallographic texture. Additionally, SPD-processed HSMs do not require chemical alterations, which might decrease the impact of physical properties such as the thermal or electrical conductivity of multidisciplinary alloys.

As shown in Fig. 1, SPD-processed HSMs combine multiple strengthening mechanisms.[2] Low-SFE and SRO trigger the formation of defects, e.g., stacking faults, twinning, GND pile-ups (to produce HDI), and the occurrence of transformation-induced plasticity (TRIP) in specific alloys. Additionally, HSMs can also combine other conventional strengthening mechanisms, including the accumulation of statistically stored dislocations (SSDs), grain refinement (Hall-Petch effect), substitutional or

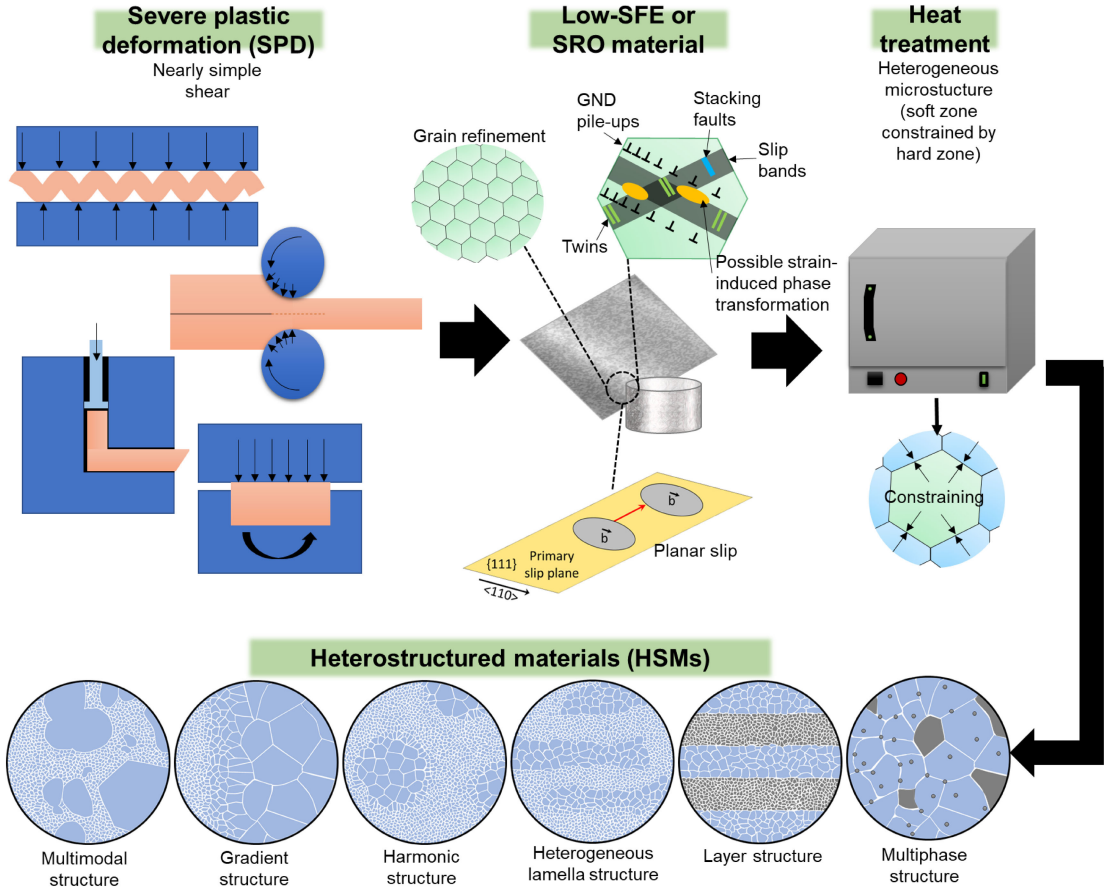

Fig. 1 SPD-based thermo-mechanical route and microstructural evolution to produce HSMs with low stacking fault energy (SFE) or short-range order (SRO).

interstitial solid solutions, or possible second-phase dispersion.

The application of short-time or low-temperature heat-treatments after SPD ensures the formation of heterogeneous structures in terms of grain size, multiphase or crystallographic texture distributions. As a result, one of the six recognized HSMs classifications can be obtained (Fig. 1): i) multimodal structure, ii) gradient structure (GS), iii) harmonic structure, iv) heterogeneous lamella structure (HLS), v) layered structure (LS), or vi) multiphase structure. Detailed reviews and compilations on the physics, microstructural and mechanical performance of HSMs can be found in the literature.[1,2,7–9] Likewise, detailed studies have been published on the physics, microstructural, and mechanical performances of SPD techniques,[3,10–20] including specific techniques, such as high-pressure torsion (HPT),[21,22] equal channel angular pressing (ECAP),[23–31] accumulative roll bonding (ARB),[32–34] and repetitive corrugation and straightening (RCS).[35,36] However, a review that explains the physics and results of combining both fields is missing from the literature.

This overview aims to serve as a basis for the fundamental features regarding microstructural evolution in HSMs produced by SPD. This overview will focus on the use of the highly reported SPD techniques; HPT, ECAP, ARB, RCS, and some surface nanostructuring techniques, mainly surface mechanical attrition treatment and shot peening. The authors expect to provide design and production guidance for new SPD-processed HSMs, as well as encourage future efforts of the scientific community through a discussion of perspectives and outstanding challenges. Finally, this overview includes current and potential multidisciplinary applications of SPD-processed HSMs that can be synergistically combined with their exceptional mechanical behavior.

2. Brief History of Severe Plastic Deformation and Heterostructured Materials

Figure 2 points out the continuous historical advancements

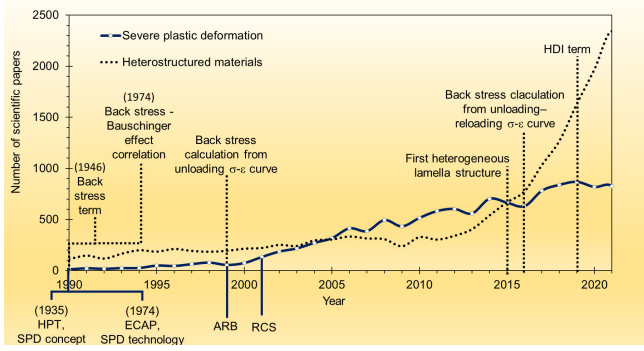

Fig. 2 Number of scientific papers published with terms “severe plastic deformation” (SPD) and “heterostructure material” (HSM) included in their title, abstract or keywords based on the Scopus database (up to August 29, 2022). The graph comprises historical developments related to SPD and HSM fields.

in SPD and HSMs fields, which have broadened their multidisciplinary applications and brought new underlying metallurgical knowledge. Regarding SPD, the development of new techniques, such as HPT,[37] ECAP,[38] ARB,[39] and RCS,[40] allowed the development of bulk nanograined (NG) and ultrafine-grained (UFG) arrangements. It's worth mentioning that while HPT research introduced the possibility of large shear stresses in confined systems, i.e., SPD as a new field,[41] the development of ECAP triggered its technological application as the first SPD technique with potential commercial use.[10] However, there are currently other SPD techniques, such as ARB and RCS, with better prospects for implementing continuous processing and producing components on a large scale. In general, SPD techniques opened the possibility: i) to introduce large strains in metallic materials by multiple deformation steps (due to almost constant geometrical dimensions before and after deformation), ii) to produce NG or UFG bulk materials with low porosity or impurities, and iii) to process higher volumes of materials than those by other techniques such as surface deposition.

The basis of HSMs started from the description of a stress field (now known as "back stress"[42]) around GND dislocations that induce hardening.[43] Later, the correlation of the Bauschinger effect[44] (difference between the applied and the reversed flow stress, causing lower compressive yield strength than the tensile yield strength, and vice versa) to the formation of back stress[45] allowed the design of precise methods based on stress-strain curves to estimate back stress.[46,47] The use of such methods broadly followed the first report on HLS material.[48] Finally, the back stress hardening was renamed as HDI hardening to include the contribution of the forward stress.[1]

SPD made it possible to produce bulk NG or UFG materials without chemical alterations, i.e., without significant impact on physical properties (e.g., electrical or thermal conductivity). Additionally, HSMs significantly relieve the typical strength–ductility trade-off associated with homogeneous materials. Due to the outstanding achievements of both SPD and HSM in mechanical metallurgy, intensive research continues in these two related areas worldwide (Fig. 2).

3. Basics of Heterostructured Materials

The outstanding mechanical properties of HSMs originated from the interactive coupling between soft and hard zones that coexist in the same microstructure. The differences in flow stress cause a heterogeneous response to the applied strain. The soft zones start deforming before the hard ones (elastic stage I in Fig. 3). Consequently, a strain gradient will be created with respect to the Frank-Read dislocation source, where the plastic strain is highest.[8] To accommodate the strain mismatch in interfaces, known as zone boundaries in HSMs, GNDs will generate from Frank-Read sources at the soft zone. Afterwards, hard zones remain elastic while soft zones start deforming plastically (stage II in Fig. 3). Both soft and hard regions remain under mutual constraining. The creation and interaction of GNDs near the zone boundaries will produce the hetero-boundary affected region (HBAR).[49]

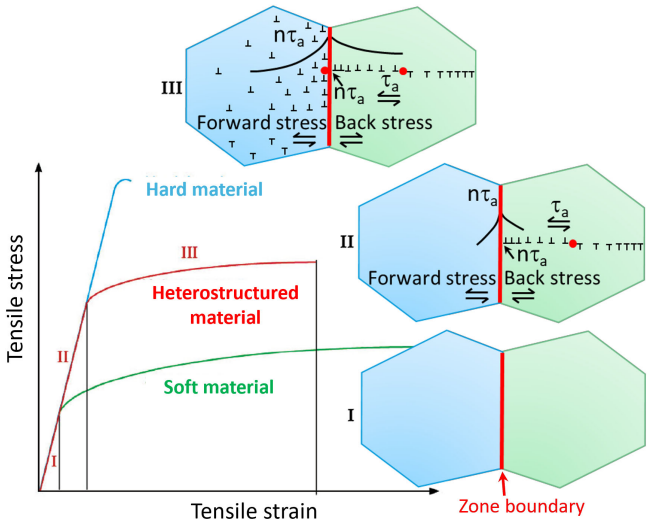

Fig. 3 Comparison of stress-strain curves for soft (green curve), hard (blue curve) and heterostructured (red curve) materials, including the representation of the three deformation stages (I, II, and III) in HSMs and their effect on dislocation behavior and stress distribution (black solid lines) near a zone boundary. Red solid circles represent the dislocation sources, while τ_a is the applied shear stress. Adapted from Ref. 9).

With increasing applied stress, the GNDs pile-up against the zone boundaries and generate long-range back stress in soft zones.[1,46] The back stress produced in such a way will act against the dislocation source to curtail the emission of more dislocations.[48] Simultaneously, the stress exerted by the head of the GND pile-up produces forward stress in hard zones.[8,50,51] The back stress strengthens soft zones, while the forward stress makes hard zones easier to deform.[7] As a result, the soft (coarse-grained) zones sustain larger deformations, while the hard ones (nano- or ultrafine-grained) act as obstacles to block the gliding of dislocations. Therefore, the HSM possesses higher strain-hardening and strengthening than that obtained in homogeneous nanostructures or coarse materials (blue and green stress-strain curves in Fig. 3).[52]

The back stress and the forward stress do not cancel each other globally, and they collectively produce the HDI strengthening to enhance yield strength and HDI strain-hardening to retain or even improve ductility. The HDI strengthening is usually negligibly small in homogeneous materials and not considered in most classical models, such as the rule of mixtures (ROM). As a result, the yield strength of HSMs is greater than that predicted by the well-known ROM,[53] i.e., greater than the strength contributions of each component weighted by their volume fractions.

Even though the HDI strengthening is dominant in HSMs, their properties still come from the synergy of multiple strengthening mechanisms. The microstructural heterogeneities in low SFE or SRO HSMs (Fig. 1), such as zone boundaries obtained from multiphase frontiers, multi-order grain sizes, twins, shear bands, stacking faults, TRIP, among others, promote the occurrence of heterogeneous deformation and diverse strengthening mechanisms.

For HSMs, the occurrence of HDI and the synergistic strengthening from the interaction and mutual constraint between the heterogeneous zones should be added to the

ROM. As a result, the modified ROM can be used as shown in eq. (1)[9,53]

$$\sigma_Y = \Delta\sigma + \frac{1}{th}\int_0^{th} \sigma(x)dx \quad (1)$$

where σ_Y is the macroscopic yield strength of the sample, $\Delta\sigma$ is the contribution of the synergistic strengthening, th is the total thickness/volume of the sample, and $\sigma(x)$ is the yield strength of each layer/zone of the sample at position x along the thickness/volume. The term $\Delta\sigma$ has a nonlinear contribution, revealing a balance between the proportion of soft and hard zones that maximizes the mechanical properties,[53] which will be discussed in section 6.

Some experimental approaches have been reported to estimate HDI stress. The HDI stress is closely related to the Bauschinger effect because they have the same origin, i.e., the GND pile-ups.[54] The Bauschinger effect refers to the difference between the applied and reversed flow stress, causing lower compressive yield strength than its tensile yield strength and vice versa.[44] The Bauschinger effect is triggered by strain gradients that can occur in heterogeneous as well as homogeneous materials. Considering the high strain gradient at zone boundaries in HSMs, the Bauschinger effect will be more significant and hence a higher HDI stress. This effect mainly influences HSMs because the strain-hardening in homogeneous materials is governed by mutual trapping and accumulation of SSDs, while strain-hardening in HSMs is controlled by HDI hardening, i.e., the pile-ups of GNDs. Some examples of the above have been reported, such as GS,[54,55] HLS,[48] alloys with soft/hard interfaces of bulk phases[56] and others with non-shearable precipitates (multiphase structured materials),[57–59] or LS passivated thin films (with film–oxide/nitride/sulfide interfaces).[60–62] This means that the contribution of HDI to the total hardening in HSMs is always higher than that of dislocation hardening.[63] This was demonstrated by the higher HDI stress due to GNDs pile-up in heterostructured Cu[55] compared to pure Cu,[64] where the Bauschinger effect was minimal.

An experimental approach to estimate the contribution of HDI stress (σ_h) during unloading–reloading loops in tensile tests is shown in eq. (2) and Fig. 4:[47]

$$\sigma_h = \frac{\sigma_r + \sigma_u}{2} \quad (2)$$

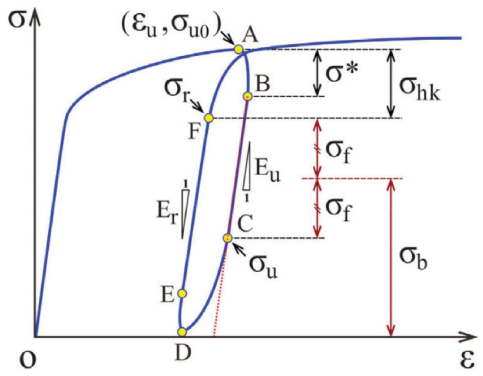

Fig. 4 The schematic of the unloading and reloading test loop to investigate the evolution of HDI stress during the tensile test.[47] The loop is used for defining the unload yielding σ_u, reload yielding σ_r, back stress σ_b and frictional stress σ_f, effective unloading Young's modulus E_u and effective reloading Young's modulus E_r.

where σ_u and σ_r are the unloading and reloading yield strength defined in the unloading–reloading stress-strain curves.[47] Equation (2) assumes reversible GND pile-up structures during the unloading–reloading process, keeping the HDI stress almost constant. This methodology reduced the measurement errors of previous models, where an arbitrary plastic strain offset was used to determine σ_u.[46,65,66] Instead, the σ_r and σ_u from eq. (2) can be estimated by the slope from the linear elastic segments of the unloading–reloading curves.[47] Some limitations and future opportunities to improve this method have been discussed in the literature.[2]

In summary, the main intrinsic characteristic of HSMs is the HDI strengthening as the major contributor to the global strengthening of the material. Due to their unique features, HSMs display a delayed necking due to continuous increase of strain-hardening, high HDI stress, and mechanical behavior that the classical ROM does not count.

4. Heterostructured Materials by Severe Plastic Deformation

This section will very briefly introduce some of the reported approaches for producing HSMs by SPD. Fundamentals of the highly studied SPD techniques, i.e., HPT,[67–69] ECAP,[70,71] ARB,[33] RCS,[40,72,73] and surface nanostructuring,[74] can be found elsewhere. In general, SPD can be implemented by simple shear (e.g., ECAP and simple shear extrusion[10,75]) and pure shear stress (e.g., cross loading, pure shear extrusion, and central areas of severe cold rolling[76,77]). In simple shear, the plastic flow is concentrated along the main direction. While in pure shear, the distortion occurs in two directions. Simple shear is the optimal deformation mode as it gives rise to fine homogeneous structures with high-angle grain boundaries (HAGBs), which could be helpful in enhancing ductility.

Bulk SPD techniques such as HPT and ECAP combined with heat-treatments can produce multimodal structures, harmonic structures, heterogeneous lamella structures, or multiphase-structured HSMs (classification shown in Fig. 1). Due to the heterogeneous nature of the strain during the first pass of the RCS technique, it does not require heat-treatment to produce multimodal structure. On the other hand, the ARB technique has been widely used to produce LS by stacking alternating plates of various materials. Lastly, the gradient structured materials, where the grain size increases gradually from the surface to the interior, are produced by surface SPD techniques.

The heat-treatments applied to the UFG or NG materials produced by SPD aims for partial recrystallization with final heterogeneous grain size distributions or thermally-induced phase transformation with final multiphase microstructures. Thus, to obtain HSMs, the most common heat-treatments on SPD-processed alloys are short-time annealing and phase reversion. The dependence of recrystallization temperature on the stress state of the material, as well as the thickness and parent phases, should be considered in the selection of heat-treatment temperature and time.

The factors influencing microstructural evolution during different SPD processing routes can be inherent to the materials or thermo-mechanical parameters. The factors inherent to the material will be discussed further in section 5. The thermo-mechanical processing parameters that control the final grain size and phase volume fractions are strain rate, equivalent strain, processing or heat-treatment temperature, and heat-treatment time.

4.1 High pressure torsion (HPT)

Due to the large applied strain, HPT introduces more severe grain refinement than ECAP, ARB, or RCS. Therefore, compared to other SPD methods, the HPT-produced UFG or nanometric materials are relatively more prone to the typical strength–ductility trade-off.[78] However, synergistic mechanical properties between the soft and hard zones in HSMs reduce the severe loss of ductility while strengthening. HSMs have been produced by combining HPT and heat-treatments[79] or by designing HPT-processed LS materials.[80–88] The first approach is based on partial recrystallization initiated from heterogeneous nucleation at defects, resulting in multimodal or HLS materials. The second approach consists of the HPT processing of stacked metal sheets of different chemical compositions with a high mechanical mismatch.

The microstructures produced by HPT become more homogeneous with increasing the number of turns of HPT. Therefore, LS materials produced by a small number of HPT turns can become multiphase structures when the layering arrangement is lost at higher strains.[81–87,89] The interface spacing is a crucial factor in the mechanical performance of LS materials.[90] The interaction of the HBAR with other strain-induced defects is expected to influence the final mechanical performance of the HPT-processed HSM (more details in section 6).

Some different uses of HPT-processed HSMs are the use of metal powders as starting materials to produce multiphase HSMs.[91] HPT-produced HSMs have also been designed for spring magnets applications, where a correlation between applied strain and magnetic properties has also been studied.[85]

4.2 Equal-channel angular pressing (ECAP)

In general, the ECAP process can produce microstructure in the nanometric size range after 4 to 5 passes, depending on the ECAP parameters.[92,93] From the fine ECAP-processed microstructures, multiphase and heterogeneous lamella structured materials can be produced by combining with subsequent heat-treatments. From section 3, heterogeneous grain sizes, texture, or phase distributions are required for at least 100% mechanical mismatch between soft and hard zones. Partial recrystallization processes are commonly used to induce large grain size disparities across the microstructure of fine-grained ECAP-processed materials. Partial recrystallization can be achieved by warm ECAP processing[94–99] or by short-time annealing post-treatments.[100] Low-temperature heat-treatments are another option to promote the formation of precipitates in the ECAP-processed material, i.e., multiphasic materials.[99,101–103] The aforementioned HSMs produced by ECAP have shown a lower strength–ductility trade-off compared to their homogeneous counterparts.[94,99–102]

Regarding physical properties, some works have focused on improving the electrochemical behavior of ECAP-processed HSMs compared with their homogeneous counterparts.[103] The improvement in their corrosion resistance has been related to less activation of galvanic pairs due to a reduced fraction of well-distributed second phases.[103] However, another report showed that the presence of fine secondary phases and high grain boundary density can be detrimental to the wear resistance of ECAP-processed HSMs.[102]

4.3 Accumulative roll bonding (ARB)

As ARB can well control the final thickness of multiple layers, numerous LS materials have been produced by this technique.[104–117] Decreasing the interface spacing in LS materials is related to the improvement of strength and ductility during uniaxial tension.[104] However, overlapping HBAR from neighboring interfaces may affect the GND pile-up formation. More details about the effect of interface spacing are presented in section 6.

Other works in cubic-structured LS materials have investigated the crystallographic texture evolution after ARB.[105,107,111] The recent findings on the texture evolution of cubic LS materials, such as stainless steel and Cu/Nb, can be found in the literature.[2,109] A study on the interface structure of ARB-elaborated HSMs can also be found elsewhere.[108]

4.4 Repetitive corrugation and straightening (RCS)

RCS results in significant grain refinement with high strengthening, as expected from the Hall-Petch relationship.[40] It is also common to obtain wide grain size distributions and non-equiaxial grain morphology after RCS processing.[35,118,119] Owing to this, RCS can provide heterostructured materials with multimodal grain size due to the heterogeneous nature of the deformation at the first pass.[72] Multimodal grain size distributions after RCS can be encouraged by the die geometry and by avoiding the 90° rotation between passes.[120] Examples of multimodal structures have been widely reported in the literature.[119,121–126] The synergistic performance of nanometric, UFG, and micrometric grains which coexist in the same structure, has been shown to increase the bulk yield strength.[121] A synergistic performance to improve electrochemical corrosion resistance and stress corrosion cracking has also been reported in wide-grain size distribution Al-7075 alloy processed by RCS.[119,121] Other works have focused on the simulation of fracture or residual stress in RCS-processed multimodal materials.[120,127–129]

4.5 Surface nanostructuring

Surface nanostructuring includes several techniques that apply large stress impacting the microstructure from a few nanometers to tens of micrometers from the surface.[130] These techniques create GS materials, i.e., they are HSMs and do not require any posterior heat-treatments. Several GS materials have been developed by surface nanostructuring techniques like peening-based processes,[131–143] surface

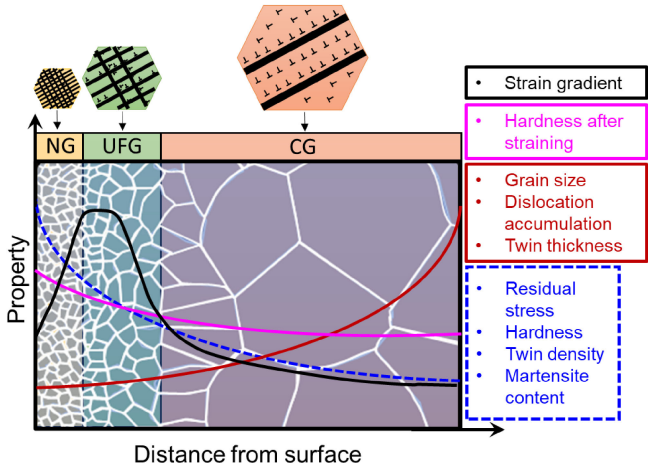

Fig. 5 Typical microstructure and features of gradient structured materials with low SFE.[2)]

mechanical attrition treatment (SMAT),[144–171)] blasting,[172–180)] ultrasonic surface deformation-based processes,[132,140,142,181–198)] and surface mechanical rolling treatment.[199–201)] From all the above, the most widely reported are SMAT and shot peening.

Surface nanostructuring techniques result in grain size distributions that changes gradually from the surface to the center of the material. Typically, NG structures can be found on the surface and micrometric grains at the center. A typical GS material is schematized in Fig. 5. The GS is typically formed by gradients in grain size, but it can also be achieved by gradient crystallographic texture or defects density.[2)] As a result, GS materials combine the virtues of a high-strength surface with a ductile center. The substantial strain disparities among layers during straining will lead to mutual constraining and the formation of GND pile-ups to accommodate the strain mismatch. Thus, a significant HDI strengthening and HDI strain-hardening will be obtained as described in previous section 3. Figure 5 shows the expected tendencies for some microstructural features and strain gradients near the NG/CG interface in GS materials. It has been shown that in GS materials, the GNDs density is maximum near the UFG (SMAT-treated)/CG interface[202)] and increases with increasing strain gradient.[203)] The same tendency of strain gradient has been observed by height contour measurements in GS materials.[204,205)] From section 3, the strain gradient is required to keep the material continuity at the interface during straining.[205)]

5. Factors Influencing Microstructural Evolution in SPD-Processed HSMs

The deformation modes strongly depend on crystal structure, SFE, initial crystallographic texture and microstructure, strain rate, stress state, and processing temperature. Out of these features, the first three are intrinsic to the material, while the latter three are processing parameters. For a clear understanding of fundamentals, the intrinsic and processing parameters affecting the microstructural evolution of SPD-processed HSMs will be discussed in separate sections. However, these parameters are interrelated and it is difficult to separate their individual contributions in practice. The critical microstructural factors to control the mechanical behavior of HSMs will be discussed in section 6.

5.1 Intrinsic parameters

5.1.1 Crystal structure

The active twin or slip systems in a material depends on the crystal structure. Thus, the microstructural response of materials to the shear stress from SPD might differ depending on their crystal structure. According to von Mises,[206)] an arbitrary deformation can be described by six terms in the strain tensor, one of them being constant due to preserved volume. Thus, five independent slip systems are necessary to preserve the continuity of a crystal during plastic deformation by slip. High-symmetry crystalline structures, like face-centered cubic (fcc) with 12 slip systems ($\{111\}\langle 110\rangle$) or body-centered cubic (bcc) with up to 48 slip systems ($\{110\}\langle 111\rangle$, $\{112\}\langle 111\rangle$, and $\{123\}\langle 111\rangle$), meet the criterion. However, due to the lack of close-packed planes in the bcc structures, thermal activation of slip systems may sometimes be necessary.

Other low-symmetry crystalline structures, such as hexagonal with only 3 slip systems (prismatic-$\{10\bar{1}0\}\langle 11\bar{2}0\rangle$ or basal-$\{0001\}\langle 11\bar{2}0\rangle$), have low plasticity at room temperature. Twin systems or preferred crystallographic orientations may allow small plasticity in hexagonal materials. The lattice parameters ratio c/a also strongly impacts the deformation mode of hexagonal materials. Thus, polycrystalline hexagonal metals, e.g., Ti, Zn, or Mg, require raising temperature to increase the number of active slip systems. Despite the low plasticity of Ti, it has been demonstrated as a very effective HSM.[48)] The limited slip systems decrease the likelihood of dislocation to cross slip among slip planes, promoting the planar slip necessary for GNDs to pile-up. As explained in section 3, GND pile-ups are the first requirement for effective HDI strengthening and HDI strain-hardening.

It should be noted that the above discussion applies to polycrystalline materials, where there is mutual constraining among neighboring grains.[207)] Since polycrystalline materials dominate most of technological applications, the case of single crystals will not be discussed here. The reader can consult comprehensive literature concerning plasticity and SPD of single crystals.[31,208–216)]

5.1.2 Factors inducing planar slip

5.1.2.1 Stacking fault energy (SFE)

SFE strongly influences the deformation mode of metals and, consequently, the generation of HDI stress. Stacking faults, bordered by Shockley partial dislocations, are planar defects with interrupted atomic arrangement sequences. The energy per unit area associated with a stacking fault determines the SFE. Low SFE materials have wide stacking faults (larger distance between partial dislocations) and promote planar slip.[217)] From section 3, planar slip encourages GND pile-ups. In contrast, high SFE materials have narrow stacking faults (smaller distance between partial dislocations), increasing the likelihood for partials to pinch in the original slip plane and be extended to an intersecting cross-slip plane.[150,217,218)]

Cross-slip decreases the likelihood of GND piling up.[7)] The difference between the planar slip and the cross-slip can

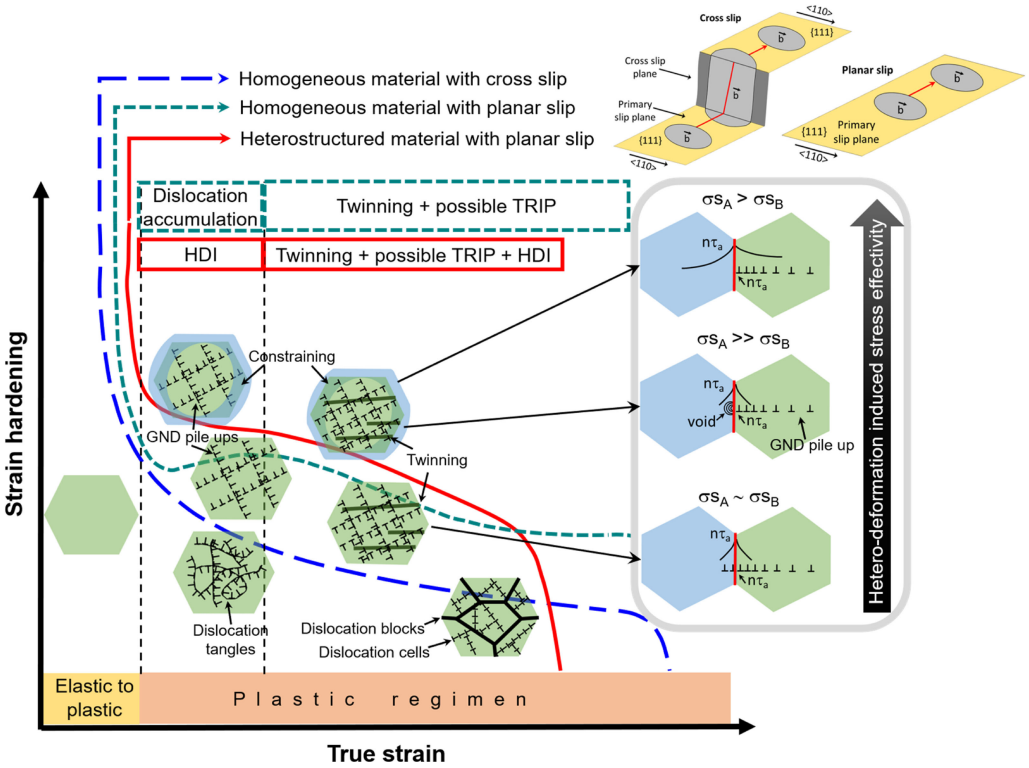

Fig. 6 Preferred strengthening mechanisms according to SFE of homogeneous and heterostructured metallic materials. σs stand for flow stress of coexisting zones A and B, τ_a is the applied shear stress, n is the number of GND in the pile-up, and $n\tau_a$ is the stress concentration. Adapted from Ref. 2).

be observed in the upper-right inserts of Fig. 6. As a result, the low SFE cubic metals deform by twinning. In contrast, cross-slip is the preferred deformation mode for medium and high SFE cubic metals. Low SFE also promotes twinning and TRIP. Generally, SFE below 20 mJ m^{-2} promotes martensitic transformation in fcc steels, while values from 12 to 45 mJ m^{-2} promote twinning.[219–222] The hexagonal metals with fewer slip systems (as mentioned in section 5.1) generally activate twinning. Some of the preferred strengthening mechanisms according to the preferred deformation mode of homogeneous and heterostructured metallic materials are shown in Fig. 6. Compared with HSMs, the homogenous medium-to-high SFE materials are governed by SSDs accumulation. The SSDs tend to group as dislocation tangles and arrange in cell blocks, which are sub-divided in incidental boundaries, also known as dislocation cells.

A detailed description of dislocation arrangement in a medium SFE Cu has been reported elsewhere.[223] As cross-slip is promoted in these materials, the contribution of GND pile-ups and HDI stress is expected to be low. At the same time, the SSDs accumulation may be significant for the strengthening and strain-hardening of the alloy. It is worth emphasizing that SSDs create short-range stress localized near the individual dislocations. Collectively, the short-range stress around the individual dislocations is canceled. In contrast, the long-range stress (back and forward) created by GND pile-ups does not cancel each other globally. Due to the above, the long-range back and forward stresses collectively produce the HDI strain-hardening and strengthening.[2]

While SFE is mainly related to chemical composition, strain rate and temperature may also influence it.[224–226] The likelihood of the transition from dislocation slip to deformation twinning, implying a decrease in SFE, increases at high pressure, high strain rates and low temperatures.[227–232] This is because the mechanically-driven grain boundary migration is limited under those conditions.[233] Besides, low temperatures also encourage dislocation accumulation, which, together with deformation twinning, tends to increase the strain hardening of alloys.[233] Other factors affecting twinning likelihood include metastable grain boundaries, stress concentrations, and favorable orientations of twin partials.[234]

It has been found that grain size has a significant effect on the deformation twinning in nanostructured metals. For fcc metals, there is an optimum grain size for twining, which can be estimated by eq. (3)[227]

$$\frac{d_m}{ln(\sqrt{2}d_m/a)} = \frac{9.69 - \nu}{253.66(1-\nu)}\frac{Ga^2}{\gamma} \tag{3}$$

where d_m is the optimum grain size, a is the lattice constant, ν is the Poisson ratio, G is the shear modulus, and γ is SFE. This equation shows that lower SFE increases the optimum grain size for twinning. In other words, low SFE makes twinning easier.

From the above, coarse and nanometric materials can show different mechanisms of deformation twinning and different kinds of deformation twins, which can be exploited by the synergistic effect of coarse and fine grains in HSMs. Coarse materials can form twins relatively easily; e.g., increasing the austenite grain size in steels has been shown to reduce the SFE.[235] It has also been reported that a higher activation stress may be required when grain size decreases further than

the optimum range for twinning.[227,236] Detailed information regarding the mechanisms of deformation twinning in nanometric metals can be found in the literature.[227,234]

It is important to mention novel strategies in multiphase HSMs with medium-to-high SFE to overcome the critical resolved stress for twinning. High SFE steels based on dual-nanoprecipitation have increased the tensile stress high enough to overcome the critical twinning stress.[237] As a result, this strategy has allowed twinning and simultaneous increment of toughness and strain hardening in high SFE steels.

5.1.2.2 Short-range order, atomic size mismatch, and shear modulus

As explained in section 5.1.2.1, avoiding cross-slip is crucial to promote the planar slip and GND pile-ups responsible for the long-range HDI stress. Besides low SFE, there are other factors that can promote the planar slip deformation mode. Those factors are based on a different combination of two Shockley partials or make the cross-slip dislocations to follow the same plane (planar slip). Those factors include high shear modulus, large atomic size mismatch, and chemical short-range order.[220,238,239]

From Taylor's theory[240] and eq. (4), a high shear modulus (G) is related to high flow stress (τ) for two parallel dislocations to overcome their elastic interactions past each other.[241] Thus, the likelihood of partials being intersected, pinched and extended to another slip plane (cross-slip) may be increased by a high G[238]

$$\tau = \frac{\alpha G b}{l} \tag{4}$$

where α is a constant of order 0.1, b is the Burgers vector, and l is the spacing between dislocations. Moreover, the ratio SFE/G is related to the spacing between dislocations and the deformation mode.[238]

Regarding atomic size mismatch, the amount of lattice distortion in a solid solution increases with the atomic size mismatch between the matrix and the alloying element.[241] The strain field increases the critical resolved shear stress and determines the dislocation interactions. Thus, higher lattice distortion also makes it difficult for the partial dislocations to be combined.

Recently, SRO has been under intensive research from the development of high-entropy alloys. In highly concentrated alloys, the head dislocation confronts a high slip resistance that is overcome while breaking the SRO. The trailing dislocations emitted from an active source face a lower slip resistance because the SRO has already been destroyed. Once the dislocations push together, the leading dislocation can overcome the slip resistance and the slip velocity and plastic deformation increases (i.e., softening effect). This deformation is localized as it is restricted to a single slip plane. The overall phenomenon leads to planar slip.[238] SRO may have a more significant impact in promoting planar slip than SFE and the critical resolved shear stress.[238] Among the examples of the SRO influence on the planar slip, a recent report on FeCrNi alloy reported planar slip despite an increased SFE due to Cu additions.[242]

Nanometric secondary phases may cause short-range clustering, also known as atomic order, which refers to local regions composed of the same atoms. If the secondary phase particles are small enough, they will be cut through by dislocations. In this case, the incoming dislocations will face cut particles with reduced strength until they are totally cut. The planar slip may encourage minor strengthening by the trailing dislocations encounter. A recent example of the above is an FeCoNi alloy with SRO nanometric intermetallic particles, which demonstrated outstanding strengthening and strain-hardening due to HDI and SSDs strengthening.[243]

5.1.3 Crystallographic texture

The importance of texture evolution in SPD process is based on two fundamental effects: 1) the plastic deformation frequently leads to preferred crystallographic orientations, and 2) the slip and twinning systems of the preferred crystallographic orientations may lead to different grain rotations.[244] As explained in section 4, ARB, RCS, HPT, and ECAP frequently lead to substantial grain refinement up to UFG or NG domains. The grain sub-division implies crystalline grain rotations. If the rotations create misorientations larger than 15°, HAGBs will be created. A similar mechanism is followed when deformation by twinning dominates. However, the twin will have a higher misorientation angle than the grain boundary.[245] Thus, the effect of the initial texture is especially important in deformation modes that are closely related to the crystalline orientation, such as twinning in hexagonal materials.

It has been identified that among the parameters affecting the texture evolution during plastic deformation, the deformation mode, the strain path, the initial texture, and the initial microstructure have a strong effect.[245] The first two parameters have been briefly described in previous sections 5.1 and 5.2. The effect of initial texture on the microstructural evolution during SPD processes is closely related to the initial texture intensity. The higher the initial texture intensity, the higher the required equivalent strain to erase its effect.[26]

For example, for many fcc alloys, 2 to 4 ECAP passes are necessary to create totally different crystallographic textures.[26] Those 2 to 4 ECAP passes coincide with the common observation of microstructural (grain size) stability in fcc alloys.[246–248] However, the texture does not necessarily remain stable after that strain; it may change continuously, forming reiteratively repeated textures when applying repeated strain paths. In some processes, such as RCS with a sinusoidal die profile, the initial texture remains nearly constant up to 4 RCS passes.[119] However, other techniques with higher equivalent strain per deformation pass, like ARB, demonstrate the ability to erase the initial texture from the first deformation pass.[122] Thus, as explained before, the texture evolution also strongly depends on the strain path and the deformation mode.

The previous general behavior has been studied mainly in homogeneous materials; the effect of the initial texture on the texture evolution after SPD of HSMs remains an important area for future research focus. To study this effect, it has been recommended to start by comparing two samples of the same material with different deformation orientations.[26] However, it should be noted that it is difficult to isolate the effect of the initial texture from the effect of other microstructural and processing parameters on the microstructural evolution.

Table 1 Main ideal texture components for plane and shear strain in fcc materials.

Plane strain		Shear strain	
Identification	*Crystal orientation {hkl}<uvw>*	*Identification*	*Crystal orientation {hkl}<uvw>*
Cube	(100)[001]	A_2^*	$(11\bar{1})[2\bar{1}1]$
Rotate cube	$(001)[1\bar{1}0]$	A_1^*	$(111)[\bar{1}\bar{1}2]$
S (S_1, S_2, S_3, S_4)	$(123)[63\bar{4}]$	A	$(1\bar{1}1)[110]$
Copper (C_1 and C_2)	$(112)[11\bar{1}]$	$\bar{A}$	$(1\bar{1}1)[110]$
Brass (B and B_2)	$(110)[1\bar{1}2]$	A	$(111)[1\bar{1}0]$
Goss (G)	(011)[100]	B	$(\bar{1}12)[110]$
α-fiber	{011}<*uvw*>	$\bar{B}$	$(\bar{1}1\bar{2})[\bar{1}\bar{1}0]$
β-fiber	B_1-S_2-C_1-S_1-B_2-S_3-C_2-S_4	C	{001}<110>
		{111}-fiber	{111}<*uvw*>
		<110>-fiber	{*hkl*}<110>

Besides, in LS materials, the crystallographic orientation relationship between layers and the morphology directionality may strongly influence texture evolution.[2)]

An example of the above is the rotations (commonly known as tilts) from the ideal texture components in Table 1, which can be widely observed in SPD-processed materials.[119)] Tilts originate from non-ideal processing conditions, such as friction between the die and the sample, die geometry, or elasto-plastic characteristics of the material.[26)] Moreover, it is difficult to isolate the effect of other microstructural factors, such as grain size, grain shape, storage stress, density of defects, etc.

Lastly, the effect of initial texture on materials with other deformation mechanisms, such as grain sliding in nanometric materials (commonly <10 nm, which coincides with the inverse Hall-Petch relationship[249)]), has not been systematically studied. Furthermore, very fine NG regions coexisting with CG regions in HSMs may have a different microstructural and mechanical effect than homogeneous NG materials. Details on the texture evolution during SPD and heat-treatments can be found in the literature.[2,27,245,250,251)]

5.2 Processing parameters

5.2.1 Stress state

The strain induced by SPD can be mainly classified as shear or plane strain.[245)] Among the SPD techniques mentioned in section 4, HPT, ECAP, and RCS (with trapezoidal die profiles) belong to shear strain mode, while ARB belongs to plane strain deformation. It is noteworthy that the slowest grain refinement is achieved by torsion.[17)]

The imposed strain mode strongly influences the final texture, but the relative intensities depend on the symmetry of the process and the applied equivalent strain. The expected texture components (crystallographic orientations) for shear and plane strain modes applied for fcc metals are shown in Table 1. The expected texture components for other crystalline structures can be found in the literature.[245)]

Changing the strain path between SPD passes may change the shearing features, activate different slip systems, and increase the grain refinement effectiveness.[223,252,253)] As described in sections 4.2 and 4.3, changing the strain path by rotations is common in ECAP and RCS processes. As a result, dislocation–dislocation interactions occur in the current slip system as well as with dislocations generated in the previous SPD passes.[223)] These interactions may generate dislocation tangles, blocks, and cells that form equiaxed grains, with increasing strain, in materials deformed by cross slip (mainly with high SFE).[252,254)] However, GND formation is triggered by the high mechanical mismatch at zone boundaries in HSMs with planar slip, where the soft zone deforms before the hard one.[5)]

5.2.2 Equivalent strain and strain rate

Increasing the equivalent strain improves the homogeneity of the final microstructure, which may be desired for HLS that require further partial recrystallization heat-treatments, but unnecessary for multimodal structured HSMs.[255)] However, it should be remarked that the use of annealing after the SPD process aims to build heterogeneous grain-size microstructures but also lower the dislocation density to improve strain hardening.

From the above, equivalent strain is a critical factor for controlling grain size and interface spacing in HSMs. The increment of equivalent shear strain increases the dislocation density, mainly SSDs for homogeneous materials and GND and SSD for HSMs. The arrangement of dislocations forms low- and then high-angle grain boundaries while increasing the strain. Thus, the increment of equivalent strain is related to higher grain refinement described mainly by grain boundary diffusion or grain boundary sliding in nanometric-grained microstructures.[256)] Higher equivalent strain also increases the defect density and residual stress. Stress accumulation at stress concentrators may provide sites for twinning nucleation,[253)] which improves strengthening and strain hardening by providing blockers for dislocation accumulation. Furthermore, twins can act as sites for phase transformation nucleation and encourage grain refinement by sub-division of coarse grains.[2,257)]

While steady microstructural (equilibrium between dynamic formation and annihilation/recovery of defects) and mechanical states typically reach at shear strain of about 100,[17)] the HPT process has gotten shear strain of over 1000.[258)] Higher microstructural and mechanical levels can be created at those HPT shear strains, as well as interesting phenomena such as atomic-scale elemental mixing.[258)] However, multiple SPD-processed HSMs have reported considerable improvement in mechanical properties within the typical strain range of SPD methods.[87,101,259–262)]

Higher defects density induced by severe shear strains may reduce the high-temperature stability of alloys. The presence of dispersed fine particles, e.g., precipitates, may help to inhibit grain growth at elevated temperatures. The thermal stability of refined microstructures has been improved by the presence of fine particles which also enhances the ductility at high strain rates (lower strain rate sensitivity).[252)]

Regarding strain rate, SPD processes are usually performed at low strain rates (of the order of $1\,mm\,s^{-1}$) to avoid temperature rise, which may cause dynamic recovery or recrystallization processes with consequent grain growth. However, dynamic recrystallization may favor ductility enhancement by encouraging HAGBs.[17)]

Increasing strain rate sensitivity is another alternative to strain hardening rate for improving ductility.[9)] Decreasing grain size in fcc and bcc systems seems to increase and decrease the strain rate sensitivity, respectively.[263–266)] This effect is usually higher in low melting point alloys. Some bcc HSMs have shown the opposite behavior of higher strain rate sensitivity with grain refinement.[267)] The authors attributed this behavior to higher dislocation density due to preferred formation of GNDs in HSMs.[267)] LS Cu/Ni have also shown an increased strain rate sensitivity at higher strain rates due to the presence of HDI, which is different behavior than the pure Cu and Ni.[268)] Higher strain rates cause an increase in GND density. However, LS Ti/Ni reported nearly constant strain rate sensitivity at higher strain rates.[269,270)] More systematic studies are required to understand the relationship between GND density and strain rate sensitivity for different classifications of HSMs.

5.2.3 Temperature, time, and pressure

Temperature and time of annealing after SPD processes can be used to control the volume fraction of recrystallized (soft) zones and their size. The formation of recrystallized (soft) zones starts at the highest defect density regions and are surrounded by non-recrystallized hard zones.[8)] Defect density, including grain boundaries, increases the storage residual energy (stress) and decreases the stability of the system. Exceptions to this effect may be alloys with restricted grain boundary mobility, such as multiphase alloys with dispersed fine secondary phases.[271,272)] Thus, recrystallization time and temperature decrease with the defect density.

Regarding pressure, it is well-reported that high-pressure processing makes the phase transformation kinetics more efficient.[17)] Besides, pressure effectively modulates interface spacing in LS materials.[273)]

6. Strength-to-Ductility Trade-Off among Different SPD Techniques

Based on different microstructural arrangements, the mechanical behavior among the six kinds of HSMs shown in Fig. 1 is expected to be different. The three most relevant microstructural factors to control are constraining (soft zones surrounded by hard zones), interface spacing, and volume fractions of soft and hard zones (Fig. 7).

The mutual constraining between soft and hard zones plays a crucial role in the mechanical behavior because it increases strain partitioning and the GND pile-ups generation. Consequently, effective constraining allows simultaneous strengthening and strain-hardening improvement. The strength–ductility relationship, given by the yield strength and uniform elongation of SPD-produced HSMs, is shown in Fig. 8.

The constraining of the soft zones embedded in the hard ones in HLS is considered the most effective method for reducing the strength–ductility trade-off among HSMs.[5)] In comparison, other HSMs, such as GS materials, have lower zone boundary density and hence lower GND pile-up formation can be expected. This is due to the fact that fine-grained zones are distributed exclusively at the surface and not in bulk. Thus, the hardening of GS materials is a function of the distance from the SPD-processed surface. In LS materials, which consists of alternating layers of different grain size or crystallographic texture, the strain partitioning may be insufficient for a significant HDI stress generation because layers are subjected to the same strain in the loading direction. However, the strain may differ in the transversal and normal directions to the loading.[5)] Thus, it is dependent on the applied stress state and a similar phenomenon may occur in GS materials. Furthermore, hard zones embedded in soft zones are the most common arrangement of multiphase materials, which is ineffective in constraining the soft zones and leads to lower HDI strengthening. Harmonic or core-shell structured materials require that the volume fractions between both zones be optimized (apparently at about 40% of the hard zone[274,275)]) to allow adequate constraints. Lastly, the multimodal structured materials, characterized by a coexistence of colonies of different order sizes, the zone boundary density is usually not maximized, reducing the HDI strengthening contribution.

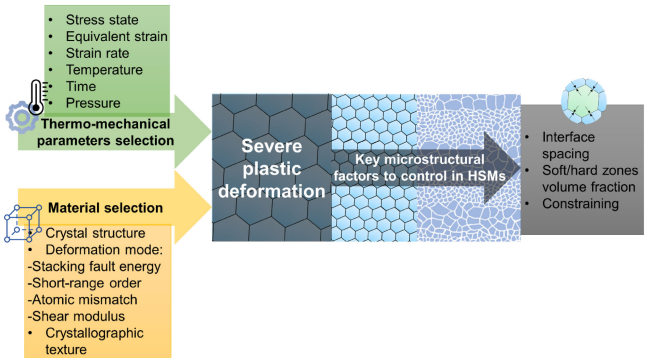

Fig. 7 Main processing parameters, materials features, and microstructural factors to consider during the design and production of SPD-processed HSMs.

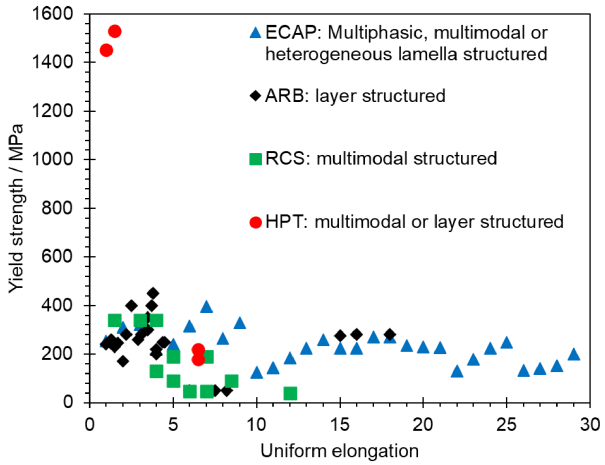

Fig. 8 Comparison of yield strength and uniform elongation among HSMs produced by different SPD techniques reported in the literature.[79,80,88,90,94–96,99,101,105,106,122,124–126,281–286)] The kinds of HSMs produced by each SPD technique are also indicated.

The HBAR, i.e., the zone affected by higher HDI stress, should also be considered in HSMs, especially in LS materials. The optimized layer thickness in LS materials should consider an interface spacing large enough to avoid overlapping the HBAR of each interface, which is estimated to be a length of about five micrometers in heterostructured Cu/bronze laminates.[104] Thus, an optimum interface spacing has been suggested to decrease the strength–ductility trade-off in LS materials. Some attempts to optimize the interface spacing have been made.[105,113] The strength–ductility trade-off has been shown to increase in layers with smaller thicknesses compared to micrometric ones.[113] This behavior may be related to the negative effect of overlapping HBAR between two interfaces when decreasing thickness. Another study correlated the crystallographic texture of LS materials of variable interfacial area fraction with its capability to accommodate deformation.[105] More systematic studies with different structures are needed to verify the effect of interface spacing on the mechanical performance of LS materials.

From eq. (1) in section 3, the synergistic strengthening does not have a linear contribution. Thus, there is an optimum fraction of coarse and fine grains to maximize the synergy between GND pile-ups and dislocation accumulation in HSMs. Some experimental approaches have been devised to optimize coarse/fine-grains fractions. The optimization has resulted in ~40% of fine grains (hard zone) for harmonic structured 304L stainless steel and copper,[274,275] ~30% of hard zone (martensite) in multiphase structured duplex stainless steel and manganese steel,[276,277] 40% of hard zone (30% nanograined and 10% nano-twinned) in an HLS 316L stainless steel,[278] and ~30% of hard zone (martensite) in a GS 304 stainless steel.[279] Besides, a maximum contribution of $\Delta\sigma$ was found by finite element method modeling in a GS interstitial-free steel with ~0.5 volume fraction of fine-grained layers.[53] Despite the optimization of mechanical properties by the abovementioned experimental and modeling approaches,[2,53,274–279] finding a mathematical model to predict the optimum fraction of zone boundaries for maximizing the contributions of HDI and other strengthening mechanisms in different HSMs remains to be explored as an active topic within the scientific community.

7. Perspectives and Outstanding Issues

HSMs are an emerging field with multiple scientific principles that challenge the understanding of conventional metallurgical literature. In addition, the fact that it is not necessary to modify the chemical composition to produce HSMs, allows maintaining or improving the physical properties simultaneously with the mechanical ones. Examples of the above are biomedical, antimicrobial,[2] magnetic[85] or catalytic[91] HSMs, among others. Thus, HSMs have great potential for industrial applications.

The applicability of HSM technology is mainly determined by scalability and the cost–benefit ratio.[5] However, SPD techniques can manufacture mainly components of small dimensions, which affects scalability. The application of continuous versions of SPD techniques to create HSMs can provide a successful route in overcoming this problem. Faraji[18] has reviewed the most promising continuous SPD methods, although they have not been used to produce HSMs. Another way to overcome this issue is by using conventional plastic deformation techniques, such as rolling, extrusion, forging, etc., to produce HSMs. Most of the HSMs with outstanding mechanical properties have been made by these traditional techniques combined with heat-treatments.[2,5] This approach can reduce the initial investment for the industrial applications of future HSMs.

Among the fundamental issues to solve in HSMs is the description of the interaction between GNDs and zone boundaries to produce HDI stress. Among the possible interaction, the GND absorption by the zone boundary, which has already been observed,[280] may affect the effectiveness of HDI stress due to changes in the number of GNDs in the pile-up. From the above, the strain gradient near the zone boundaries and its relationship with GND pile-up density should be revisited. Besides, the contribution of SFE and SRO in promoting planar slip, which is necessary for the formation of GND pile-ups and HDI stress (section 3), should be systematically investigated. It is also recommended to explore and compare the effectivity of HDI stress to reduce the strength–ductility trade-off in materials with different crystal structures. Some recent reviews have described a detailed description of the fundamental issues that must be overcome in HSMs.[2,5]

Furthermore, modeling and simulation of abnormal grain growth during partial recrystallization processes, defects interactions, optimization of the volume fractions of soft/hard zones, and stress and strain gradient distributions are necessary for accurate designs of HSMs and increasing their industrial scalability. Finally, it is imperative to include the theory of HDI strengthening and HDI strain-hardening in textbooks so that the new insights reach the younger generation and encourage future efforts to clarify multiple fundamentals of HSMs.

Acknowledgments

This review was supported by the Ministry of Science and Technology of China (2021YFA1200202), the National Natural Science Foundation of China (11988103), the Hong Kong Research Grants Council (GRF-11214121), the Hong Kong Institute for Advanced Study of City University of Hong Kong, and the Programa de Apoyo a la Investigación y el Posgrado (PAIP-50009223) of Facultad de Química of Universidad Nacional Autónoma de México. MN would like to acknowledge the Asia-Oceania Neutron Scattering Association (AONSA) for the award of the AONSA Young Research Fellowship (YRF-2022).

REFERENCES

1) Y. Zhu and X. Wu: Mater. Res. Lett. **7** (2019) 393–398.
2) L. Romero-Resendiz, M. El-Tahawy, T. Zhang, M.C. Rossi, D.M. Marulanda-Cardona, T. Yang, V. Amigo-Borras, Y. Huang, H. Mirzadeh, I.J. Beyerlein, J.C. Huang, T.G. Langdon and Y.T. Zhu: Mater. Sci. Eng. R **150** (2022) 100691.
3) R.Z. Valiev, B. Straumal and T.G. Langdon: Annu. Rev. Mater. Res. **52** (2022) 357–382.
4) B. Gao, Q. Lai, Y. Cao, R. Hu, L. Xiao, Z. Pan, N. Liang, Y. Li, G. Sha, M. Liu, H. Zhou, X. Wu and Y. Zhu: Sci. Adv. **6** (2020) eaba8169.

5) Y. Zhu and X. Wu: Prog. Mater. Sci. **131** (2023) 101019.
6) R.Z. Valiev, I.V. Alexandrov, Y.T. Zhu and T.C. Lowe: J. Mater. Res. **17** (2002) 5–8.
7) Y. Zhu, K. Ameyama, P.M. Anderson, I.J. Beyerlein, H. Gao, H.S. Kim, E. Lavernia, S. Mathaudhu, H. Mughrabi, R.O. Ritchie, N. Tsuji, X. Zhang and X. Wu: Mater. Res. Lett. **9** (2021) 1–31.
8) Y. Zhu: Metall. Mater. Trans. A **52** (2021) 4715–4726.
9) X. Wu and Y. Zhu: *Heterostructured Materials: Novel Materials with Unprecedented Mechanical Properties*, 1st edn., (Jenny Stanford, 2021).
10) V. Segal: Materials **11** (2018) 1175.
11) R. Valiev: Nat. Mater. **3** (2004) 511–516.
12) R.Z. Valiev, R.K. Islamgaliev and I.V. Alexandrov: *Bulk Nanostructured Materials from Severe Plastic Deformation*, vol. 45, (2000).
13) R.N. Harsha, V. Mithun Kulkarni and B. Satish Babu: Mater. Today Proc. **5** (2018) 22340–22349.
14) Y.T. Zhu and T.G. Langdon: JOM **56** (2004) 58–63.
15) G. Faraji, H.S. Kim and H.T. Kashi: Sev. Plast. Deform. (2018) 19–36.
16) F. Khodabakhshi, M. Mohammadi and A.P. Gerlich: J. Mater. Sci. **56** (2021) 15513–15537.
17) K. Edalati *et al.*: Mater. Res. Lett. **10** (2022) 163–256.
18) G. Faraji and H. Torabzadeh: Mater. Trans. **60** (2019) 1316–1330.
19) Y. Estrin and A. Vinogradov: Acta Mater. **61** (2013) 782–817.
20) P. Veena, D.M. Yadav and C.N. Kumar: Int. J. Sci. Res. Sci. Eng. Technol. **3** (2017) 336–343.
21) K. Edalati and Z. Horita: Mater. Sci. Eng. A **652** (2016) 325–352.
22) A.P. Zhilyaev and T.G. Langdon: Prog. Mater. Sci. **53** (2008) 893–979.
23) R.Z. Valiev and T.G. Langdon: Prog. Mater. Sci. **51** (2006) 881–981.
24) A. Gupta, B. Chandrasekhar and K.K. Saxena: Mater. Today Proc. **45** (2021) 5602–5607.
25) N. Sadasivan, M. Balasubramanian and B.R. Rameshbapu: J. Manuf. Process. **59** (2020) 698–726.
26) I.J. Beyerlein and L.S. Tóth: Prog. Mater. Sci. **54** (2009) 427–510.
27) L.S. Tóth: Adv. Eng. Mater. **5** (2003) 308–316.
28) S.S. Murugan: Int. J. Mod. Stud. Mech. Eng. **3** (2017) 6–14.
29) M. Furukawa, Z. Horita, M. Nemoto and T.G. Langdon: J. Mater. Sci. **36** (2001) 2835–2843.
30) M.F. Erinosho and E.T. Akinlabi: Lect. Notes Eng. Comput. Sci. **2224** (2016) 719–723.
31) W. Han, S. Li, S. Wu and Z. Zhang: Mater. Sci. Forum **633–634** (2010) 511–525.
32) S.M. Ghalehbandi, M. Malaki and M. Gupta: Appl. Sci. **9** (2019) 3627–3659.
33) N. Tsuji, Y. Saito, S.H. Lee and Y. Minamino: Adv. Eng. Mater. **5** (2003) 338–344.
34) A. Arun and L. Poovazhagan: Mater. Sci. Forum **979** (2020) 84–88.
35) B.R. Sunil: Mater. Manuf. Process. **30** (2015) 1262–1271.
36) A.K. Gupta, T.S. Maddukuri and S.K. Singh: Prog. Mater. Sci. **84** (2016) 403–462.
37) P.W. Bridgman: Phys. Rev. **48** (1935) 825–847.
38) V.M. Segal: Physical Technical Institute Academy of Sciences of Buelorussia, (1974).
39) N. Tsuji, Y. Saito, H. Utsunomiya and S. Tanigawa: Scr. Mater. **40** (1999) 795–800.
40) Y.T. Zhu, H. Jiang, J. Huang and T.C. Lowe: Metall. Mater. Trans. A **32** (2001) 1559–1562.
41) P.W. Bridgman: J. Appl. Phys. **8** (1937) 328–336.
42) A.S. Nowick and E.S. Machlin: J. Appl. Phys. **18** (1947) 79–87.
43) A. Kochendörfer: Z. Phys. **108** (1938) 244–264.
44) J. Bauschinger: Zivilingenieur **27** (1881) 289–348.
45) P.M. Hazzledine and P.B. Hirsch: Philos. Mag. **30** (1974) 1331–1351.
46) X. Feaugas: Acta Mater. **47** (1999) 3617–3632.
47) M. Yang, Y. Pan, F. Yuan, Y. Zhu and X. Wu: Mater. Res. Lett. **4** (2016) 145–151.
48) X. Wu, M. Yang, F. Yuan, G. Wu, Y. Wei, X. Huang and Y. Zhu: Proc. Natl. Acad. Sci. USA **112** (2015) 14501–14505.
49) C.X. Huang, Y.F. Wang, X.L. Ma, S. Yin, H.W. Höppel, M. Göken, X.L. Wu, H.J. Gao and Y.T. Zhu: Mater. Today **21** (2018) 713–719.
50) F. Mompiou, D. Caillard, M. Legros and H. Mughrabi: Acta Mater. **60** (2012) 3402–3414.
51) H. Mughrabi: Philos. Mag. **86** (2006) 4037–4054.
52) Z. Cheng, H. Zhou, Q. Lu, H. Gao and L. Lu: Science **362** (2018) eaau1925.
53) X.L. Wu, P. Jiang, L. Chen, J.F. Zhang, F.P. Yuan and Y.T. Zhu: Mater. Res. Lett. **2** (2014) 185–191.
54) X. Hu, S. Jin, H. Zhou, Z. Yin, J. Yang, Y. Gong, Y. Zhu, G. Sha and X. Zhu: Metall. Mater. Trans. A **48** (2017) 3943–3950.
55) X. Liu, F. Yuan, Y. Zhu and X. Wu: Scr. Mater. **150** (2018) 57–60.
56) J. He, L. Chen, Z. Guo, H. Zhi, S. Antonov and Y. Su: Mater. Sci. Eng. A **793** (2020) 139835.
57) R.E. Stoltz and R.M. Pelloux: Metall. Trans. A **7** (1976) 1295–1306.
58) A.P. Reynolds and J.S. Lyons: Metall. Mater. Trans. A **28** (1997) 1205–1211.
59) M.X. Yang, F.P. Yuan, Q.G. Xie, Y.D. Wang, E. Ma and X.L. Wu: Acta Mater. **109** (2016) 213–222.
60) C. Zhou and R. Lesar: Comput. Mater. Sci. **54** (2012) 350–355.
61) Y. Xiang and J.J. Vlassak: Scr. Mater. **53** (2005) 177–182.
62) Y. Xiang and J.J. Vlassak: Acta Mater. **54** (2006) 5449–5460.
63) X. Wu and Y. Zhu: Mater. Res. Lett. **5** (2017) 527–532.
64) O.B. Pedersen, L.M. Brown and W.M. Stobbs: Acta Metall. **29** (1981) 1843–1850.
65) J.I. Dickson, J. Boutin and L. Handfield: Mater. Sci. Eng. **64** (1984) L7–L11.
66) B. Fournier, M. Sauzay, C. Caës, M. Noblecourt and M. Mottot: Mater. Sci. Eng. A **437** (2006) 183–196.
67) A.P. Zhilyaev, T.R. McNelley and T.G. Langdon: J. Mater. Sci. **42** (2007) 1517–1528.
68) P.H.R. Pereira, R.B. Figueiredo, P.R. Cetlin and T.G. Langdon: Mater. Sci. Eng. A **631** (2015) 201–208.
69) D.J. Lee, E.Y. Yoon, D.H. Ahn, B.H. Park, H.W. Park, L.J. Park, Y. Estrin and H.S. Kim: Acta Mater. **76** (2014) 281–293.
70) Y.T. Zhu and T.C. Lowe: Mater. Sci. Eng. A **291** (2000) 46–53.
71) V.M. Segal: Mater. Sci. Eng. A **271** (1999) 322–333.
72) N. Thangapandian, S. Balasivanandha Prabu and K.A. Padmanabhan: Mater. Sci. Eng. A **649** (2016) 229–238.
73) Y. Zhu, J. Huang, H. Jiang and T. Lowe: Second Global Symposium on Innovations in Materials Processing and Manufacturing: Sheet Materials, (2001) pp. 175–182.
74) X. Li, L. Lu, J. Li, X. Zhang and H. Gao: Nat. Rev. Mater. **5** (2020) 706–723.
75) N. Pardis and R. Ebrahimi: Mater. Sci. Eng. A **527** (2010) 6153–6156.
76) V.M. Segal: Mater. Sci. Eng. A **338** (2002) 331–344.
77) F. Rahimi and A.R. Eivani: Mater. Sci. Eng. A **626** (2015) 423–431.
78) T. Sakai, A. Belyakov, R. Kaibyshev, H. Miura and J.J. Jonas: Prog. Mater. Sci. **60** (2014) 130–207.
79) B. Schuh, R. Pippan and A. Hohenwarter: Mater. Sci. Eng. A **748** (2019) 379–385.
80) Q. Huo, Y. Chen, B. Gao, Y. Liu, M. Liu, X. Chen and H. Zhou: Acta Metall. Sin. (English Lett.) **36** (2023) 343–351.
81) R.R. Mulyukov, G.F. Korznikova, K.S. Nazarov, R.K. Khisamov, S.N. Sergeev, R.U. Shayachmetov, G.R. Khalikova and E.A. Korznikova: Acta Mech. **232** (2021) 1815–1828.
82) D. Hernández-Escobar, Z.U. Rahman, H. Yilmazer, M. Kawasaki and C.J. Boehlert: Philos. Mag. **99** (2019) 557–584.
83) D. Hernández-Escobar, M. Kawasaki and C.J. Boehlert: Int. Mater. Rev. **67** (2022) 231–265.
84) M. Kawasaki, J.K. Han, D.H. Lee, J.I. Jang and T.G. Langdon: J. Mater. Res. **33** (2018) 2700–2710.
85) L. Weissitsch, M. Stückler, S. Wurster, P. Knoll, H. Krenn, R. Pippan and A. Bachmaier: Crystals **10** (2020) 1026.
86) M. Kawasaki, S.H. Jung, J.M. Park, J. Lee, J.I. Jang and J.K. Han: Adv. Eng. Mater. **22** (2020) 1900483.
87) D. Hernández-Escobar, J. Marcus, J.K. Han, R.R. Unocic, M. Kawasaki and C.J. Boehlert: Mater. Sci. Eng. A **771** (2020) 138578.
88) X. Chen, L. Xiao, Y. Liu, M. Xu, T. Xu, B. Gao, Z. Hu and H. Zhou: Vacuum **179** (2020) 109568.
89) D. Hernández-Escobar, R.R. Unocic, M. Kawasaki and C.J. Boehlert: J. Alloy. Compd. **831** (2020) 154891.
90) X. Ma, C. Huang, J. Moering, M. Ruppert, H.W. Höppel, M. Göken,

J. Narayan and Y. Zhu: Acta Mater. **116** (2016) 43–52.
91) S. Akrami, M. Watanabe, T.H. Ling, T. Ishihara, M. Arita, M. Fuji and K. Edalati: Appl. Catal. B **298** (2021) 120566.
92) Y. Iwahashi, Z. Horita, M. Nemoto and T.G. Langdon: Acta Mater. **46** (1998) 3317–3331.
93) V.V. Stolyarov, Y. Theodore Zhu, I.V. Alexandrov, T.C. Lowe and R.Z. Valiev: Mater. Sci. Eng. A **299** (2001) 59–67.
94) L.B. Tong, J.H. Chu, W.T. Sun, Z.H. Jiang, D.N. Zou, S.F. Liu, S. Kamado and M.Y. Zheng: J. Magnes. Alloy. **9** (2021) 1007–1018.
95) H. Liu, L. Ye, K. Ren, C. Sun, X. Zhuo, K. Yan, J. Ju, J. Jiang, F. Xue and J. Bai: J. Mater. Res. Technol. **21** (2022) 5032–5044.
96) K. Ren, K. Zhang, Y. Zhang, J. Ju, K. Yan, J. Jiang, A. Ma, F. Xue, J. Bai and H. Liu: Mater. Sci. Eng. A **826** (2021) 141990.
97) J. Wang, P. Chen, L. Meng and L. Jin: Adv. Eng. Mater. **24** (2022) 2101581.
98) Z. Yang, A. Ma, B. Xu, J. Jiang, H. Wu and J. Sun: Mater. Sci. Eng. A **841** (2022) 143023.
99) Y. Fu, J. Sun, Z. Yang, B. Xu, J. Han, Y. Chen, J. Jiang and A. Ma: Mater. Charact. **165** (2020) 110398.
100) H. Ran, R.R. Jin, Y.F. Wang, M.S. Wang, Q. He, F.J. Guo, Y. Wen and C.X. Huang: Mater. Sci. Eng. A **807** (2021) 140906.
101) J. Sun, B. Xu, Z. Yang, X. Zhuo, J. Han, Y. Wu, D. Song, H. Liu, J. Jiang and A. Ma: Mater. Charact. **164** (2020) 110341.
102) B. Xu, J. Sun, Z. Yang, J. Han, D. Song, J. Jiang and A. Ma: Scanning **2020** (2020) 4873286.
103) Z. Yang, A. Ma, B. Xu, J. Jiang and J. Sun: Corros. Sci. **187** (2021) 109517.
104) X. Ma, C. Huang, J. Moering, M. Ruppert, H.W. Höppel, M. Göken, J. Narayan and Y. Zhu: Acta Mater. **116** (2016) 43–52.
105) I.J. Beyerlein, N.A. Mara, J.S. Carpenter, T. Nizolek, W.M. Mook, T.A. Wynn, R.J. McCabe, J.R. Mayeur, K. Kang, S. Zheng, J. Wang and T.M. Pollock: J. Mater. Res. **28** (2013) 1799–1812.
106) K. Wu, H. Chang, E. Maawad, W.M. Gan, H.G. Brokmeier and M.Y. Zheng: Mater. Sci. Eng. A **527** (2010) 3073–3078.
107) M.Z. Quadir, N. Najafzadeh and P.R. Munroe: Mater. Des. **93** (2016) 467–473.
108) J. Wang, K. Kang, R.F. Zhang, S.J. Zheng, I.J. Beyerlein and N.A. Mara: JOM **64** (2012) 1208–1217.
109) N.A. Mara and I.J. Beyerlein: J. Mater. Sci. **49** (2014) 6497–6516.
110) P. Chekhonin, J. Scharnweber, M. Scharnweber, C.G. Oertel, T. Hausöl, H.W. Höppel, J. Jaschinski, T. Marr and W. Skrotzki: Cryst. Res. Technol. **48** (2013) 532–537.
111) J.S. Carpenter, S.C. Vogel, J.E. Ledonne, D.L. Hammon, I.J. Beyerlein and N.A. Mara: Acta Mater. **60** (2012) 1576–1586.
112) D.C.C. Magalhães, S.A.E. Huitron, J.M.C. Marrero, O.M. Cintho, A.M. Kliauga and V.L. Sordi: Adv. Eng. Mater. **25** (2023) 2201092.
113) H.W. Höppel, M. Westermeyer, F. Kümmel and M. Göken: Adv. Eng. Mater. **22** (2020) 2000145.
114) M.Z. Quadir, O. Al-Buhamad, K.D. Lau, R. Quarfoth, L. Bassman, P.R. Munroe and M. Ferry: Int. J. Mater. Res. **100** (2009) 1705–1714.
115) P. Chekhonin, B. Beausir, J. Scharnweber, C.G. Oertel, T. Hausöl, H.W. Höppel, H.G. Brokmeier and W. Skrotzki: Acta Mater. **60** (2012) 4661–4671.
116) M.C. Chen, H.C. Hsieh and W. Wu: J. Alloy. Compd. **416** (2006) 169–172.
117) S.H.S. Ebrahimi, K. Dehghani, J. Aghazadeh, M.B. Ghasemian and S. Zangeneh: Mater. Sci. Eng. A **718** (2018) 311–320.
118) J. Jenix Rino, S. Balasivanandha Prabu and K.A. Padmanabhan: Arch. Civ. Mech. Eng. **18** (2018) 280–290.
119) L. Romero-Resendiz, M. Hernández, J.M. Cabrera, S. Elizalde, I.A. Figueroa, A. Covelo and G. Gonzalez: J. Appl. Res. Technol. **20** (2022) 284–297.
120) P. Tajdary, L. Morin, C. Braham and G. Gonzalez: Int. J. Mater. Form. **14** (2021) 1403–1416.
121) L. Romero-Resendiz, V. Amigo-Borras, A. Vicente-Escuder, S. Elizalde, J.M. Cabrera, D. Pineda-Ruiz, I.A. Figueroa and G. Gonzalez: J. Mater. Res. Technol. **15** (2021) 4564–4572.
122) L. Romero-Resendiz, J.M. Cabrera, S. Elizalde, V. Amigó-Borrás, I.A. Figueroa and G. Gonzalez: J. Mater. Res. Technol. **18** (2022) 1281–1294.
123) M. Ezequiel, S. Elizalde, J.M. Cabrera, J. Picas, I.A. Figueroa, I. Alfonso and G. Gonzalez: Materials **13** (2020) 633.
124) E.E. Alvarado, I.A. Figueroa and G. Gonzalez: Phys. Met. Metallogr. **121** (2020) 1319–1325.
125) M. Ezequiel, I.A. Figueroa, S. Elizalde, J.M. Cabrera, C. Braham, L. Morin and G. Gonzalez: J. Mater. Res. Technol. **9** (2020) 1941–1947.
126) S. Elizalde, M. Ezequiel, I.A. Figueroa, J.M. Cabrera, C. Braham and G. Gonzalez: Metals **10** (2020) 489–500.
127) P. Tajdary, L. Morin, L. Romero-resendiz, M.B. Gorji and C. Braham: Int. J. Solids Struct. **248** (2022) 111640.
128) L. Morin, C. Braham, P. Tajdary, R. Seddik and G. Gonzalez: Mech. Mater. **158** (2021) 103882.
129) P. Tajdary, L. Morin, C. Braham and G. Gonzalez: Exp. Mech. **62** (2022) 1349–1362.
130) T. Grosdidier and M. Novelli: Mater. Trans. **60** (2019) 1344–1355.
131) E.R. de los Rios, A. Walley, M.T. Milan and G. Hammersley: Int. J. Fatigue **17** (1995) 493–499.
132) H. Lee, D. Kim, J. Jung, Y. Pyoun and K. Shin: Corros. Sci. **51** (2009) 2826–2830.
133) T. Wang, J. Yu and B. Dong: Surf. Coat. Technol. **200** (2006) 4777–4781.
134) Y. He, K.B. Yoo, H. Ma and K. Shin: Mater. Lett. **215** (2018) 187–190.
135) J.S. Li, W.D. Gao, Y. Cao, Z.W. Huang, B. Gao, Q.Z. Mao and Y.S. Li: Adv. Eng. Mater. **20** (2018) 1800402.
136) Y.F. Al-Obaid: Eng. Fract. Mech. **51** (1995) 19–25.
137) S. Pour-Ali, A.R. Kiani-Rashid and A. Babakhani: Vacuum **144** (2017) 152–159.
138) M. Jayalakshmi, P. Huilgol, B.R. Bhat and K. Udaya Bhat: Surf. Coat. Technol. **344** (2018) 295–302.
139) M.A.S. Torres and H.J.C. Voorwald: Int. J. Fatigue **24** (2002) 877–886.
140) Y. He, K. Li, I.S. Cho, C.S. Lee, I.G. Park and K. Shin: Microsc. Microanal. **20** (2014) 844–845.
141) Y. Zou, Z. Sang, Q. Wang, T. Li, D. Li and Y. Li: Mater. Sci. **26** (2020) 161–167.
142) B.N. Mordyuk, Y.V. Milman, M.O. Iefimov, G.I. Prokopenko, V.V. Silberschmidt, M.I. Danylenko and A.V. Kotko: Surf. Coat. Technol. **202** (2008) 4875–4883.
143) X. Wang, Y.S. Li, Q. Zhang, Y.H. Zhao and Y.T. Zhu: J. Mater. Sci. Technol. **33** (2017) 758–761.
144) A.M. Gatey, S.S. Hosmani, R.K.P. Singh and S. Suwas: Adv. Mater. Res. **794** (2013) 238–247.
145) S. Bajda, W. Ratuszek, M. Krzyzanowski and D. Retraint: Surf. Coat. Technol. **329** (2017) 202–211.
146) Q. He, W. Wei, M. Wang, F. Guo, Y. Zhai, Y. Wang and C. Huang: Nanomaterials **11** (2021) 2356–2367.
147) T.-T. Chen, J. Wang, Y. Zhang, P. Jiang, F.-P. Yuan, P.-D. Han and X.-L. Wu: Mater. Sci. Eng. A **837** (2022) 142727.
148) S. Qin, M. Yang, F. Yuan and X. Wu: Nanomaterials **11** (2021) 1856.
149) T. Balusamy, S. Kumar and T.S.N. Sankara Narayanan: Corros. Sci. **52** (2010) 3826–3834.
150) H.W. Zhang, Z.K. Hei, G. Liu, J. Lu and K. Lu: Acta Mater. **51** (2003) 1871–1881.
151) X.H. Chen, J. Lu, L. Lu and K. Lu: Scr. Mater. **52** (2005) 1039–1044.
152) T. Roland, D. Retraint, K. Lu and J. Lu: Mater. Sci. Eng. A **445–446** (2007) 281–288.
153) T. Fu, Z.F. Zhou, Y.M. Zhou, X.D. Zhu, Q.F. Zeng, C.P. Wang, K.Y. Li and J. Lu: Surf. Coat. Technol. **207** (2012) 555–564.
154) T. Bai, P. Chen and K. Guan: Mater. Sci. Eng. A **561** (2013) 498–506.
155) T. Balusamy, T.S.N. Sankara Narayanan, K. Ravichandran, I.S. Park and M.H. Lee: Corros. Sci. **74** (2013) 332–344.
156) M. Novelli, J.J. Fundenberger, P. Bocher and T. Grosdidier: Appl. Surf. Sci. **389** (2016) 1169–1174.
157) Q. He, Y.F. Wang, M.S. Wang, F.J. Guo, Y. Wen and C.X. Huang: Mater. Sci. Eng. A **780** (2020) 139146 Contents.
158) D. Bernoulli, S.C. Cao, J. Lu and M. Dao: Surf. Coat. Technol. **339** (2018) 14–19.
159) K. Lu and J. Lu: Mater. Sci. Eng. A **375–377** (2004) 38–45.
160) T. Roland, D. Retraint, K. Lu and J. Lu: Scr. Mater. **54** (2006) 1949–1954.
161) Y. Wu, B. Guelorget, Z. Sun, R. Déturche and D. Retraint: Mater.

Charact. **155** (2019) 109788 Contents.
162) Y. Sun: Tribol. Int. **57** (2013) 67–75.
163) L. Chen and X.L. Wu: Mater. Sci. Forum **682** (2011) 123–130.
164) A. Chen, J. Liu, H. Wang, J. Lu and Y.M. Wang: Mater. Sci. Eng. A **667** (2016) 179–188.
165) Z. Sun, D. Retraint, T. Baudin, A.L. Helbert, F. Brisset, M. Chemkhi, J. Zhou and P. Kanouté: Mater. Charact. **124** (2017) 117–121.
166) T. Balusamy, S. Kumar and T.S.N. Sankara Narayanan: Trans. Indian Inst. Met. **64** (2011) 507–511.
167) J. Zhou, Z. Sun, P. Kanouté and D. Retraint: Int. J. Fatigue **103** (2017) 309–317.
168) X.H. Yang, W.Z. Dui and G. Liu: Key Eng. Mater. **353–358** (2007) 1810–1813.
169) S. Bahl, P. Shreyas, M.A. Trishul, S. Suwas and K. Chatterjee: Nanoscale **7** (2015) 7704–7716.
170) B. Thangaraj, S.N.T.S. Nellaiappan, R. Kulandaivelu, M.H. Lee and T. Nishimura: ACS Appl. Mater. Interfaces **7** (2015) 17731–17747.
171) Y. Hao, B. Deng, C. Zhong, Y. Jiang and J. Li: J. Iron Steel Res. Int. **16** (2009) 68–72.
172) D. Kanesan, M.E. Mohyaldinn, N.I. Ismail, D. Chandran and C.J. Liang: J. Nat. Gas Sci. Eng. **65** (2019) 267–274.
173) M. Faller, S. Buzzi and O.V. Trzebiatowski: Mater. Corros. **56** (2005) 373–378.
174) Z. Makama, I. Doble, D. Nicolson, M.E. Webb, I.B. Beech, S.A. Campbell and J.R. Smith: Trans. Inst. Met. Finish. **89** (2011) 237–243.
175) W. Morton, S. Green, A.E.W. Rennie and T.N. Abram: Innov. Dev. Virtual Phys. Prototyp. - Proc. 5th Int. Conf. Adv. Res. Rapid Prototyp., (2012) pp. 503–509.
176) H. Begg, M. Riley and H. de Villiers Lovelock: J. Therm. Spray Technol. **25** (2016) 12–20.
177) N.L. Tshimanga, G.A. Combrink and M.W. Kalenga: Mater. Today Proc. **38** (2021) 544–548.
178) X.Y. Wang and D.Y. Li: Electrochim. Acta **47** (2002) 3939–3947.
179) M. Multigner, S. Ferreira-Barragáns, E. Frutos, M. Jaafar, J. Ibáñez, P. Marín, M.T. Pérez-Prado, G. González-Doncel, A. Asenjo and J.L. González-Carrasco: Surf. Coat. Technol. **205** (2010) 1830–1837.
180) B. Yu, E.M. Davis, R.S. Hodges, R.T. Irvin and D.Y. Li: Nanotechnology **19** (2008) 335101.
181) X.H. Zhao, D.W. Nie, D.S. Xu, Y. Liu and C.H. Hu: Tribol. Trans. **62** (2019) 189–197.
182) H. Wang, G. Song and G. Tang: Mater. Sci. Eng. A **662** (2016) 456–467.
183) D. Liu, D. Liu, X. Zhang, C. Liu, A. Ma, X. Xu and W. Zhang: Int. J. Fatigue **131** (2020) 105340.
184) Q. Zhang, Z. Hu, W. Su, H. Zhou, C. Liu, Y. Yang and X. Qi: Surf. Coat. Technol. **321** (2017) 64–73.
185) Y. Liu, J. Sun, Y. Fu, B. Xu, B. Li, S. Xu, P. Huang, J. Cheng, Y. Han, J. Han and G. Wu: Addit. Manuf. **48** (2021) 102373.
186) G. Liu, J. Lu and K. Lu: Mater. Sci. Eng. A **286** (2000) 91–95.
187) B.N. Mordyuk, G.I. Prokopenko, M.A. Vasylyev and M.O. Iefimov: Mater. Sci. Eng. A **458** (2007) 253–261.
188) X. Yang, X. Wang, X. Ling and D. Wang: Results Phys. **7** (2017) 1412–1421.
189) C. Ye, A. Telang, A.S. Gill, S. Suslov, Y. Idell, K. Zweiacker, J.M.K. Wiezorek, Z. Zhou, D. Qian, S.R. Mannava and V.K. Vasudevan: Mater. Sci. Eng. A **613** (2014) 274–288.
190) Y. He, K. Wang and K. Shin: J. Mater. Sci. **56** (2021) 4858–4870.
191) M. Novelli, P. Bocher and T. Grosdidier: Mater. Charact. **139** (2018) 197–207.
192) H.B. Wang, X.H. Yang, H. Li, G.L. Song and G.Y. Tang: J. Mater. Res. **33** (2018) 3827–3840.
193) J. Liu, C. Wang, W. Zhang, T. Xia, X. Zhang, T. Liang, T. Ahmad and B. Yang: Mater. Sci. Technol. **35** (2019) 907–915.
194) D. Liu, D. Liu, X. Zhang, C. Liu and N. Ao: Mater. Sci. Eng. A **726** (2018) 69–81.
195) C. Li, R. Zhu, X. Zhang, P. Huang, X. Wang and X. Wang: Surf. Coat. Technol. **383** (2020) 125280.
196) C. Wang, J. Han, J. Zhao, Y. Song, J. Man, H. Zhu, J. Sun and L. Fang: Coatings **9** (2019) 276.
197) Y.X. Liu, H. Chen, R.Z. Wang, Y.F. Jia, X.C. Zhang, Y. Cui and S.T. Tu: Int. J. Fatigue **147** (2021) 106170.
198) X. Han, C. Li, C. Chen, X. Zhang and H. Zhang: Nanomaterials **11** (2021) 1769.
199) H.W. Huang, Z.B. Wang, J. Lu and K. Lu: Acta Mater. **87** (2015) 150–160.
200) M.X. Shen, K.J. Rong, D.J. Liu, G.Y. Xiong, D.H. Ji and X.G. Wang: Surf. Topogr. Metrol. Prop. **8** (2020) 035009.
201) L. Carneiro, X. Wang and Y. Jiang: Int. J. Fatigue **134** (2020) 105469.
202) Y. Samih, B. Beausir, B. Bolle and T. Grosdidier: Mater. Charact. **83** (2013) 129–138.
203) K. Lu: Nat. Rev. Mater. **1** (2016) 16019.
204) Y.F. Wang, M.S. Wang, X.T. Fang, F.J. Guo, H.Q. Liu, R.O. Scattergood, C.X. Huang and Y.T. Zhu: Int. J. Plast. **123** (2019) 196–207.
205) X. Wu, P. Jiang, L. Chen, F. Yuan and Y.T. Zhu: Proc. Natl. Acad. Sci. USA **111** (2014) 7197–7201.
206) R. Von Mises: Z. Angew. Math. Mech. **8** (1928) 161–185.
207) G. Yang and S.J. Park: Materials **12** (2019) 2003.
208) E. Tohidlou and A. Bertram: Mech. Mater. **114** (2017) 30–39.
209) P. Wagner, O. Engler and K. Lücke: Acta Metall. Mater. **43** (1995) 3799–3812.
210) M. Furukawa, Z. Horita and T.G. Langdon: Mater. Sci. Eng. A **503** (2009) 21–27.
211) G.Y. Deng, C. Lu, L.H. Su, X.H. Liu and A.K. Tieu: Mater. Sci. Eng. A **534** (2012) 68–74.
212) P. Šedá, A. Jäger, P. Lejček and P. Romano Triguero: Philos. Mag. **94** (2014) 1095–1111.
213) W.Z. Han, Z.F. Zhang, S.D. Wu and S.X. Li: Scr. Mater. **59** (2008) 385–386.
214) Y. Fukuda, K. Oh-ishi, M. Furukawa, Z. Horita and T.G. Langdon: Mater. Sci. Eng. A **420** (2006) 79–86.
215) E.G. Astafurova, M.S. Tukeeva, G.G. Maier, E.V. Melnikov and H.J. Maier: Mater. Sci. Eng. A **604** (2014) 166–175.
216) M. Niewczas: Mater. Sci. Technol. **30** (2014) 739–757.
217) A. Das: Metall. Mater. Trans. A **47** (2016) 748–768.
218) T.H. Simm: Crystals **8** (2018) 212.
219) J. Lu, L. Hultman, E. Holmström, K.H. Antonsson, M. Grehk, W. Li, L. Vitos and A. Golpayegani: Acta Mater. **111** (2016) 39–46.
220) I. Gutierrez-Urrutia and D. Raabe: Acta Mater. **59** (2011) 6449–6462.
221) B.C. De Cooman, Y. Estrin and S.K. Kim: Acta Mater. **142** (2018) 283–362.
222) S. Allain, J.P. Chateau, O. Bouaziz, S. Migot and N. Guelton: Mater. Sci. Eng. A **387–389** (2004) 158–162.
223) J.Y. Huang, Y.T. Zhu, H. Jiang and T.C. Lowe: Acta Mater. **49** (2001) 1497–1505.
224) J. Wan, S. Chen and Z. Xu: Sci. China Ser. E Technol. Sci. **44** (2001) 345–352.
225) P.C.J. Gallagher: Metall. Trans. **1** (1970) 2429–2461.
226) S.F. Liu, Y. Wu, H.T. Wang, J.Y. He, J.B. Liu, C.X. Chen, X.J. Liu, H. Wang and Z.P. Lu: Intermetallics **93** (2018) 269–273.
227) Y.T. Zhu, X.Z. Liao and X.L. Wu: Prog. Mater. Sci. **57** (2012) 1–62.
228) X. An, S. Ni, M. Song and X. Liao: Adv. Eng. Mater. **22** (2020) 1900479.
229) S. Mahajan and D.F. Williams: Int. Mater. Rev. **18** (1973) 43–61.
230) M. Naeem, H. He, F. Zhang, H. Huang, S. Harjo, T. Kawasaki, B. Wang, S. Lan, Z. Wu, F. Wang, Y. Wu, Z. Lu, Z. Zhang, C.T. Liu and X.L. Wang: Sci. Adv. **6** (2020) eaax4002.
231) M. Naeem, H. He, S. Harjo, T. Kawasaki, W. Lin, J.J. Kai, Z. Wu, S. Lan and X.L. Wang: Acta Mater. **221** (2021) 117371.
232) M. Naeem, H. Zhou, H. He, S. Harjo, T. Kawasaki, S. Lan, Z. Wu, Y. Zhu and X.L. Wang: Appl. Phys. Lett. **119** (2021) 131901.
233) X. Zhou, X.Y. Li and K. Lu: Scr. Mater. **153** (2018) 6–9.
234) Y.T. Zhu, X.Z. Liao and X.L. Wu: JOM **60** (2008) 60–64.
235) O.A. Zambrano: J. Eng. Mater. Technol. **138** (2016) 041010.
236) Q. Yu, Z.W. Shan, J. Li, X. Huang, L. Xiao, J. Sun and E. Ma: Nature **463** (2010) 335–338.
237) Z. Wang, W. Lu, F. An, M. Song, D. Ponge, D. Raabe and Z. Li: Nat. Commun. **13** (2022) 3598.
238) V. Gerold and H.P. Karnthaler: Acta Metall. **37** (1989) 2177–2183.
239) S.I. Hong and C. Laird: Acta Metall. Mater. **38** (1990) 1581–1594.
240) G.I. Taylor: Proc. R. Soc. London, Ser. A **145** (1934) 362–387.

241) D. Hull and D.J. Bacon: *Introduction to Dislocations*, 5th edn., (Butterworth-Heinemann, Oxford, 2011).
242) H. Cho, S. Kim, Y. Cho and S. Kim: Mater. Charact. **190** (2022) 112052.
243) T. Yang, Y.L. Zhao, Y. Tong, Z.B. Jiao, J. Wei, J.X. Cai, X.D. Han, D. Chen, A. Hu, J.J. Kai, K. Lu, Y. Liu and C.T. Liu: Science **362** (2018) 933–937.
244) D.A. Hughes and N. Hansen: Acta Mater. **45** (1997) 3871–3886.
245) S. Suwas and S. Mondal: Mater. Trans. **60** (2019) 1457–1471.
246) L. Romero-Resendiz, I.A. Figueroa, C. Reyes-Ruiz, J.M. Cabrera, C. Braham and G. Gonzalez: Mater. Charact. **152** (2019) 44–57.
247) O. Renk and R. Pippan: Mater. Trans. **60** (2019) 1270–1282.
248) J. Gubicza: Mater. Trans. **60** (2019) 1230–1242.
249) S. Takeuchi: Scr. Mater. **44** (2001) 1483–1487.
250) H. Azzeddine, D. Bradai, T. Baudin and T.G. Langdon: Prog. Mater. Sci. **125** (2022) 100886.
251) S. Li, I.J. Beyerlein and M.A.M. Bourke: Mater. Sci. Eng. A **394** (2005) 66–77.
252) M. Furukawa, Z. Horita, M. Nemoto and T.G. Langdon: Mater. Sci. Eng. A **324** (2002) 82–89.
253) Y. Wang, M. Chen, F. Zhou and E. Ma: Nature **419** (2002) 912–915.
254) N. Tsuji, N. Kamikawa and B.L. Li: Mater. Sci. Forum **539–543** (2007) 2837–2842.
255) W. Skrotzki: Mater. Trans. **60** (2019) 1331–1343.
256) T.C. Lowe and R.Z. Valiev: JOM **52** (2000) 27–28.
257) N. Nakada, H. Ito, Y. Matsuoka, T. Tsuchiyama and S. Takaki: Acta Mater. **58** (2010) 895–903.
258) K. Edalati: Mater. Trans. **60** (2019) 1221–1229.
259) J.K. Han, J. Il Jang, T.G. Langdon and M. Kawasaki: Mater. Trans. **60** (2019) 1131–1138.
260) Y. Chen, J. Nie, F. Wang, H. Yang, C. Wu, X. Liu and Y. Zhao: J. Alloy. Compd. **815** (2020) 152285.
261) M. Ebrahimi and Q. Wang: J. Mater. Res. Technol. **19** (2022) 4381–4403.
262) Y. Wang, M. Yang, X. Ma, M. Wang, K. Yin, A. Huang and C. Huang: Mater. Sci. Eng. A **727** (2018) 113–118.
263) Q. Wei: J. Mater. Sci. **42** (2007) 1709–1727.
264) G.M. Cheng, W.W. Jian, W.Z. Xu, H. Yuan, P.C. Millett and Y.T. Zhu: Mater. Res. Lett. **1** (2013) 26–31.
265) G.M. Cheng, W.Z. Xu, W.W. Jian, H. Yuan, M.H. Tsai, Y.T. Zhu, Y.F. Zhang and P.C. Millett: J. Mater. Res. **28** (2013) 1820–1826.
266) Q. Wei, S. Cheng, K.T. Ramesh and E. Ma: Mater. Sci. Eng. A **381** (2004) 71–79.
267) F. Yuan, P. Chen, Y. Feng, P. Jiang and X. Wu: Mech. Mater. **95** (2016) 71–82.
268) Z. Fu, Z. Zhang, L. Meng, B. Shu, Y. Zhu and X. Zhu: Mater. Sci. Eng. A **726** (2018) 154–159.
269) J. Shi, M.Z. Wei, Y.J. Ma, L.J. Xu, Z.H. Cao and X.K. Meng: Mater. Sci. Eng. A **648** (2015) 31–36.
270) J. Shi, Z.H. Cao and J.G. Zheng: Mater. Sci. Eng. A **680** (2017) 210–213.
271) S. Komura, Z. Horita, M. Furukawa, M. Nemoto and T.G. Langdon: J. Mater. Res. **15** (2000) 2571–2576.
272) P.B. Berbon, S. Komura, A. Utsunomiya, Z. Horita, M. Furukawa, M. Nemoto and T.G. Langdon: Mater. Trans. JIM **40** (1999) 772–778.
273) S. Pei, Z. Wang and J. Xia: Mater. Des. **213** (2022) 110363.
274) Z. Zhang, S.K. Vajpai, D. Orlov and K. Ameyama: Mater. Sci. Eng. A **598** (2014) 106–113.
275) C. Sawangrat, S. Kato, D. Orlov and K. Ameyama: J. Mater. Sci. **49** (2014) 6579–6585.
276) K. Park, M. Nishiyama, N. Nakada, T. Tsuchiyama and S. Takaki: Mater. Sci. Eng. A **604** (2014) 135–141.
277) M. Calcagnotto, Y. Adachi, D. Ponge and D. Raabe: Acta Mater. **59** (2011) 658–670.
278) J. Li, Y. Cao, B. Gao, Y. Li and Y. Zhu: J. Mater. Sci. **53** (2018) 10442–10456.
279) X.L. Wu, M.X. Yang, F.P. Yuan, L. Chen and Y.T. Zhu: Acta Mater. **112** (2016) 337–346.
280) H. Zhou, C. Huang, X. Sha, L. Xiao, X. Ma, H.W. Höppel, M. Göken, X. Wu, K. Ameyama, X. Han and Y. Zhu: Mater. Res. Lett. **7** (2019) 376–382.
281) S.E. Mousavi, A. Sonboli, M. Meratian, M. Amirnejad, S.H.M. Azghandi and P. Munroe: Mater. Sci. Eng. A **802** (2021) 140654.
282) C. Reyes-Ruiz, C.G. Figueroa, G. González and A. Ortiz: Phys. Met. Metallogr. **122** (2021) 504–514.
283) B. Xu, J. Sun, J. Han, Z. Yang, H. Zhou, L. Xiao, S. Xu, Y. Han, A. Ma and G. Wu: Corros. Sci. **194** (2022) 109924.
284) M. Heydari Vini and M. Sedighi: Can. Metall. Q. **57** (2018) 160–167.
285) M. Sedighi, P. Farhadipour and M. Heydari Vini: JOM **68** (2016) 3193–3200.
286) D. Rahmatabadi, M. Tayyebi, A. Sheikhi and R. Hashemi: Mater. Sci. Eng. A **734** (2018) 427–436.